Nonrelativistic full-folding model of nucleon elastic scattering at intermediate energies

H. F. Arellano
Department of Physics and Astronomy, University of Georgia, Athens, Georgia 30602

F. A. Brieva
Department of Physics and Astronomy, University of Georgia, Athens, Georgia 30602
and Departamento de Física, Facultad de Ciencias Físicas y Matemáticas, Universidad de Chile, Casilla 487-3, Santiago, Chile

W. G. Love
Department of Physics and Astronomy, University of Georgia, Athens, Georgia 30602
(Received 10 November 1989)

Nonrelativistic full-folding optical model potentials for nucleon elastic scattering have been calculated and applied to proton scattering on ^{16}O and ^{40}Ca at energies between 135 and 500 MeV. The optical potentials were calculated in momentum space by folding the mixed target density with the off-energy-shell free t matrix derived from the Paris nucleon-nucleon potential. The energy dependence and knockon exchange terms of the t matrix were included explicitly. Significant differences were observed between observables calculated from the full-folding model and conventional $t\rho$ approximations to it. At proton energies near and below $\sim$400 MeV, the full-folding model provides a substantial improvement in the description of the data compared to $t\rho$ approximations. These results demonstrate the importance of accurate treatments of the off-energy-shell properties of effective interactions as well as the mixed density in calculating nonrelativistic optical potentials for intermediate energy nucleon scattering. Exploratory calculations at 500 MeV together with those at lower energies suggest the need for an improved description of the nucleon-nucleon interaction at higher energies.

I. INTRODUCTION

Since its introduction, the nuclear optical model has been recognized as one of the simplest and yet most powerful theoretical approaches to the complex problem of describing and understanding the physics involved in nucleon-nucleus scattering. If this approach is to be successful at a microscopic level, the calculation of optical potentials must adequately represent the interplay between target ground-state properties, the effective nucleon-nucleon (NN) interaction, and medium correlations. The complicated structure of microscopic optical potentials has led to the development of several well-established, though limited, approximations for studying nucleon-nucleus scattering. Most of these approximations result in an optical potential which is calculated by folding the target density with a local NN effective interaction; we shall refer to this scheme as the standard folding model. At low and intermediate energies, the most successful[1-3] variation of the standard folding model uses a complex, energy- and density-dependent effective interaction calculated from a realistic NN potential. At higher energies, where further approximations are better justified, the NN effective interaction is taken to be the free NN t matrix evaluated on the energy shell. This leads to a factorized $t\rho$ structure[4] for the optical potential in momentum space.

An element common to all variants of the standard folding model is that of somehow averaging the energy and momentum dependence of the effective interaction in order to obtain a simplified force which facilitates its use in subsequent calculations. In the nuclear medium, these averaging procedures introduce a medium dependence into the effective force beyond that present in the true off-shell interaction. As a result, the separation and identification of the dominant effects at different energies such as medium corrections and off-shell contributions cannot be carried out unambiguously within the standard folding model.

Extensive applications of the standard folding model of the nucleon-nucleus optical potential to nucleon elastic scattering have met with varying degrees of success. In the energy region below $\sim$100 MeV, where medium corrections are treated within the framework of a local density approximation, the calculated potentials provide a reasonable qualitative description of cross section and analyzing power data. At these energies, the agreement between measured and calculated results can be improved notably if a renormalization is allowed for each component of the optical potential.[5] There is, however, no physical basis for such a procedure other than to improve the fit to the data. Even at higher energies the $t\rho$ model has difficulties describing satisfactorily some features of the data. Although the introduction of relativistic de-

grees of freedom through the relativistic $t\rho$ approximation[4,6–8] often improves the agreement with the data significantly, an alternative mechanism may be found in a correct treatment of the off-shell degrees of freedom of the force within a nonrelativistic framework.[9] The present study addresses the latter approach.

One of the primary purposes of developing a microscopic theory of elastic scattering is that of learning about the target ground-state properties, nuclear correlations, and the characteristics of the basic internucleon force in the medium. This requires that the theory consider explicitly each effect without unnecessary *ab initio* simplification. Only then can we have a reliable account of each of the effects contributing to the optical potential and a base line from which further corrections may be introduced.

In this paper we review some aspects of the formalism of the nonrelativistic full-folding model of the optical potential and present results from applications of the model to elastic nucleon scattering. Emphasis is on an explicit treatment of the off-shell behavior of the NN t matrix, its energy dependence, and the associated knockon exchange terms as well as on an explicit treatment of the mixed density of the target ground state. A brief account of a few results has been reported previously.[9] We shall limit the present applications to energies between 135 and 500 MeV, although the approach we present can be applied over a wider range of energies. This restriction is based on two main considerations. First, the NN potentials which provide the best descriptions of NN scattering data have been developed over a limited range of energies, thus setting a limit for the region of applicability of the full-folding model. Second, we have assumed that intrinsic medium corrections, such as those arising from Pauli blocking, are small enough so that the free off-shell NN t matrix represents a good first approximation to the effective NN interaction. Actually, medium corrections, usually associated with Fermi averaging within the local-density approximation, are naturally accounted for in the full-folding framework by treating explicitly the energy and momentum dependence of the NN t matrix for each NN collision. Recent calculations[9] of the nucleon-nucleus optical potential in the 200–300 MeV region suggest that most of the measured observables can be reasonably well reproduced by treating the full off-shell characteristics of the effective force explicitly, and that in a full-folding framework, medium corrections *may* be less important at intermediate energies than found previously using local $t\rho$ models.[1–3]

The outline of this paper is as follows. In Sec. II we present the assumptions leading to the full-folding model and derive an explicit expression for it in a momentum representation. In Sec. III we provide some details of the calculations of the full-folding potential, discuss the treatment of the Coulomb potential when calculating observables for proton elastic scattering, and briefly examine the sensitivity of the scattering observables to the single-particle model used for calculating the optical potential. In Sec. IV we compare results from the full-folding model with measured observables for proton scattering on ^{16}O and ^{40}Ca, as well as with results from alternative $t\rho$ approximations to the optical potential. In Sec. V we present a summary and draw the main conclusions of the present work.

II. THE FULL-FOLDING MODEL

One of the underlying assumptions in the formulation of the nonrelativistic full-folding optical potential is the existence of a bare NN potential which gives a reasonable description of the existing data for the two-nucleon system. In practice, well established NN potential models have been developed for energies up to around 400 MeV; work on extending the models to higher energies[10] is an active area of research. In light of this, we focus primarily on incident nucleon energies near and below 400 MeV, where the most definitive conclusions may be drawn. Calculations at 500 MeV were made to explore differences between the full-folding approach and alternative approximations to it.

Given an $(A+1)$ particle Hamiltonian H_{A+1}, the description of the elastic scattering of a nucleon from an A-particle target relies on the reduction of the many-body Hamiltonian to an effective one-body Hamiltonian $h(E)$ which correctly describes the elastic scattering channel

$$h(E)=K_0+U(E)\ , \tag{2.1}$$

where K_0 is the projectile kinetic energy and $U(E)$ is the optical potential. There are essentially two alternative approaches to construct $U(E)$. One of them is based on the very transparent theories of Kerman, McManus, and Thaler[11] (KMT) and Watson,[12–14] where the emphasis is on the global properties of the target nucleus, its excitation spectrum, and its coupling to the projectile. This scheme is most directly applicable when the incident projectile is distinguishable from the target nucleons, although the fully antisymmetrized theory for nucleon scattering is available,[14–16] at least formally. One shortcoming of the KMT and Watson approaches is their inadequacy for describing low-energy nuclear scattering due to the slow rate of convergence of the resulting multiple-scattering series.[17] Moreover, the asymmetric treatment of the scattered and struck nucleons precludes a systematic reduction of the many-body propagators to two-body propagators of interacting pairs in the nuclear field consistent with the Pauli principle. The alternative approach is based on a many-body description of nuclear reactions, where the theory is formulated explicitly in terms of single-particle degrees of freedom and accounts naturally for the indistinguishability of all participating nucleons.[18] This latter scheme has been successful in describing nucleon elastic scattering in the region below 200 MeV. In order to understand and interpret explicit off-shell effects in the optical $U(E)$, we review briefly the derivation of the full-folding model at intermediate energies. At these energies we shall see how the alternative approaches lead to the same result for the optical potential.

A. Theoretical framework

In the KMT and Watson theories, the H_{A+1} Hamiltonian is written as

$$H_{A+1}=H_A+K_0+V \ , \tag{2.2}$$

where H_A is the target Hamiltonian and V is the nucleon-nucleus coupling, namely

$$V=\sum_{i=1}^{A} v_{0i} \ , \tag{2.3}$$

with v_{0i} the bare internucleon potential between the incident proton and the ith nucleon in the target. Three-body and higher-order forces are not considered here.

The optical potential for a particle of incident kinetic energy E [Eq. (2.1)] can be written, in a momentum representation, as

$$U(\mathbf{k}',\mathbf{k};E)=\langle \mathbf{k}';\Phi_0|T(E+E_0)|\mathbf{k};\Phi_0\rangle_{\mathcal{A}} \ , \tag{2.4}$$

that is, the antisymmetrized ($\mathcal{A}$) matrix elements of an $(A+1)$-body transition matrix evaluated at the total energy $E+E_0$ in the initial state. The Φ_n are eigenstates of the A-particle target Hamiltonian H_A,

$$H_A|\Phi_n\rangle=E_n|\Phi_n\rangle \ , \tag{2.5}$$

and E_0 is the ground-state energy. The nucleon-nucleus T matrix satisfies

$$T(E+E_0)=V+V\Lambda(E+E_0)T(E+E_0) \ , \tag{2.6}$$

where $\Lambda(\Omega)$ is the $(A+1)$-particle propagator defined by

$$\Lambda(\Omega)=\frac{Q}{\Omega-\mathcal{H}_{QQ}+i\eta} \ . \tag{2.7}$$

Here Q represents the $(A+1)$-particle projection operator off the target ground state

$$Q=\sum_{n\neq 0}\int d\mathbf{k}|\mathbf{k};\Phi_n\rangle\langle\mathbf{k};\Phi_n| \ , \tag{2.8}$$

and $\mathcal{H}_{QQ}$ represents the asymptotic Hamiltonian projected off the ground state

$$\mathcal{H}_{QQ}=Q(K_0+H_A)Q \ . \tag{2.9}$$

Considering that the projectile-target potential V can be expressed as in Eq. (2.3), a formal solution to Eq. (2.6) for T can be written as

$$T(\Omega)=\sum_{i=1}^{A} T^{(i)}(\Omega) \ , \tag{2.10}$$

with $T^{(i)}$ satisfying

$$T^{(i)}(\Omega)=\tau_i(\Omega)+\sum_{j\neq i}\tau_i(\Omega)\Lambda(\Omega)T^{(j)}(\Omega) \ , \tag{2.11}$$

and τ_i being a solution of

$$\tau_i(\Omega)=v_{0i}+v_{0i}\Lambda(\Omega)\tau_i(\Omega) \ . \tag{2.12}$$

Note that τ_i is an $(A+1)$-body operator. Equation (2.11) for $T^{(i)}$ generates the multiple-scattering series for the optical potential. The leading term of this series defines the full-folding model,

$$U(\mathbf{k}',\mathbf{k};E)=\sum_{i=1}^{A}\langle \mathbf{k}';\Phi_0|\tau_i(E+E_0)|\mathbf{k};\Phi_0\rangle_{\mathcal{A}} \ . \tag{2.13}$$

The problem of calculating the τ_i operator is still prohibitive due to the presence of the many-body propagator Λ in Eq. (2.12). Indeed, this propagator can be expressed as

$$\Lambda(\Omega)=\sum_{n\neq 0}\int d\mathbf{p}\frac{|\mathbf{p};\Phi_n\rangle\langle\mathbf{p};\Phi_n|}{\Omega-(p^2/2m+E_n)+i\eta} \ . \tag{2.14}$$

To simplify Λ we neglect recoil effects and assume a single-particle description of the target states with the projectile interacting with only one target nucleon at a time while the remaining nucleons act as spectators. Therefore, in the denominator we set

$$\Omega=E+E_0, \quad E_0-E_n\approx\epsilon_\alpha-\epsilon_\beta, \quad \epsilon_\alpha<\epsilon_F,\epsilon_\beta>\epsilon_F \ , \tag{2.15}$$

with ϵ_α and ϵ_β representing single-particle energies below and above the Fermi energy of the target ϵ_F. Consequently, the many-body propagator can be related to a propagator effective in the two-particle space,

$$\langle \mathbf{k}'_0\mathbf{k}'_1,\ldots,\mathbf{k}'_A|\Lambda(E+E_0)|\mathbf{k}_0\mathbf{k}_1,\ldots,\mathbf{k}_A\rangle \approx\delta(\mathbf{k}'_2-\mathbf{k}_2)\cdots\delta(\mathbf{k}'_A-\mathbf{k}_A)\langle \mathbf{k}'_0\mathbf{k}'_1|G(E+\epsilon_\alpha)|\mathbf{k}_0\mathbf{k}_1\rangle \ , \tag{2.16}$$

where

$$G(E+\epsilon_\alpha)=\sum_{\beta}\int d\mathbf{p}\frac{|\mathbf{p};\varphi_\beta\rangle\langle\mathbf{p};\varphi_\beta|}{E+\epsilon_\alpha-p^2/2m-\epsilon_\beta+i\eta}\Theta(\epsilon_\beta-\epsilon_F) \ , \tag{2.17}$$

In the above equation φ_β represents the target single-particle state corresponding to the single-particle energy ϵ_β. It is worth noting the asymmetry between the incident and bound target propagation; while the target nucleon propagates in the nuclear field, the incoming particle propagates freely in intermediate states. This is characteristic of the KMT approach. The symmetry can be restored if one includes the self-energy of the incident particle as suggested by the many-body approach. In this work we neglect those medium effects associated with self-energy corrections and Pauli blocking by setting the single-particle energy equal to its free value and the Θ function to unity. Therefore,

$$G(E+\epsilon_\alpha)\approx G_0(E+\epsilon_\alpha)=\int d\mathbf{k}_\beta\int d\mathbf{p}\frac{|\mathbf{p};\mathbf{k}_\beta\rangle\langle\mathbf{p};\mathbf{k}_\beta|}{E+\epsilon_\alpha-p^2/2m-k_\beta^2/2m+i\eta} \ , \tag{2.18}$$

which corresponds to a free two-body propagator for the pair. At intermediate energies we expect this approximation to be reasonable; in any case, it provides a framework within which explicit medium corrections and other effects may be introduced in a relatively transparent way.

In the approximation given by Eq. (2.18) for G, the matrix elements of τ_1 say, can be expressed as

$$\langle \mathbf{k}'_0 k'_1, \ldots, \mathbf{k}'_A | \tau_1(E+E_0) | \mathbf{k}_0 \mathbf{k}_1, \ldots, \mathbf{k}_A \rangle_{\mathcal{A}} \approx \delta(\mathbf{k}'_2 - \mathbf{k}_2) \cdots \delta(\mathbf{k}'_A - \mathbf{k}_A) \langle \mathbf{k}'_0 \mathbf{k}'_1 | \tilde{t}_1(E+\epsilon_\alpha) | \mathbf{k}_0 \mathbf{k}_1 \rangle_{\mathcal{A}} , \tag{2.19}$$

with $\tilde{t}_i$ the free two-nucleon t matrix given by

$$\tilde{t}_i(\omega) = v_{0i} + v_{0i} G_0(\omega) \tilde{t}_i(\omega) . \tag{2.20}$$

Therefore, the leading term for the optical potential can be expressed as

$$U(\mathbf{k}',\mathbf{k};E) = \sum_{\epsilon_\alpha < \epsilon_F} \int d\mathbf{p}' \int d\mathbf{p} \varphi^\dagger_\alpha(\mathbf{p}') \times \langle \mathbf{k}'\mathbf{p}' | \tilde{t}(E+\epsilon_\alpha) | \mathbf{k}\mathbf{p} \rangle_{\mathcal{A}} \varphi_\alpha(\mathbf{p}) , \tag{2.21}$$

where $\tilde{t}$ corresponds to any of the t matrices $\tilde{t}_i$ defined in Eq. (2.20). Eq. (2.21) defines the full-folding optical potential. This result is consistent with that obtained in the many-body approach, where, in the absence of medium corrections, the many-body medium-corrected reaction matrix (or g matrix) reduces to the free t matrix for the interacting pair.

Taking into account total momentum conservation for the interacting nucleon pair, the two-body t matrix $\tilde{t}$ can be expressed in terms of a reduced one-body t matrix $\hat{t}$ acting between states of relative momenta:

$$\langle \mathbf{k}'\mathbf{p}' | \tilde{t}(E+\epsilon_\alpha) | \mathbf{k}\mathbf{p} \rangle_{\mathcal{A}} = \delta(\mathbf{k}'+\mathbf{p}'-\mathbf{k}-\mathbf{p}) \left\langle \tfrac{1}{2}(\mathbf{k}'-\mathbf{p}') \left| \hat{t}\left[E+\epsilon_\alpha - \frac{(\mathbf{p}+\mathbf{k})^2}{2M} \right] \right| \tfrac{1}{2}(\mathbf{k}-\mathbf{p}) \right\rangle_{\mathcal{A}} , \tag{2.22}$$

where M is the total mass of the pair and $\hat{t}$ satisfies

$$\hat{t}(z) = v + v \frac{1}{z - K + i\eta} \hat{t}(z) . \tag{2.23}$$

Here K represents the relative kinetic energy operator and v any v_{0i}. The assumption of momentum conservation in the two-body subsystem expressed by Eq. (2.22) for $\tilde{t}$ allows us to simplify Eq. (2.21) for the full-folding potential and obtain

$$U(\mathbf{k}',\mathbf{k};E) = \sum_{\epsilon_\alpha < \epsilon_F} \int d\mathbf{Q} \varphi^\dagger_\alpha(\mathbf{Q}-\mathbf{k}') \langle \mathbf{k}' - \tfrac{1}{2}\mathbf{Q} | \hat{t}\left[E+\epsilon_\alpha - \frac{Q^2}{2M} \right] | \mathbf{k} - \tfrac{1}{2}\mathbf{Q} \rangle_{\mathcal{A}} \varphi_\alpha(\mathbf{Q}-\mathbf{k}) , \tag{2.24}$$

where the integration is now over the NN center-of-mass momentum $\mathbf{Q}$. The major difficulty with calculating $U(\mathbf{k}',\mathbf{k};E)$ as given by Eq. (2.24) is that of evaluating the three-dimensional integral while retaining the complicated energy and momentum dependence of the t matrix. The method used to evaluate $U(\mathbf{k}',\mathbf{k};E)$ is described in the following sections.

B. Explicit expressions

When evaluating the full-folding integral occurring in Eq. (2.24) it is convenient to use an alternative set of vectors to $(\mathbf{k}',\mathbf{k},\mathbf{Q})$ defined by

$$\mathbf{q} = \mathbf{k} - \mathbf{k}', \quad \mathbf{K} = \tfrac{1}{2}(\mathbf{k}+\mathbf{k}'), \quad \mathbf{P} = \mathbf{Q} - \mathbf{K} \tag{2.25}$$

and to let $\mathbf{P}$ be the new variable of integration. Figure 1 shows the geometrical relationship between the different vectors. In addition to the defining equations for $\mathbf{q}$, $\mathbf{K}$, and $\mathbf{Q}$, it is useful to note that

$$\mathbf{p}' = \mathbf{P} + \tfrac{1}{2}\mathbf{q}, \quad \mathbf{p} = \mathbf{P} - \tfrac{1}{2}\mathbf{q}, \quad \mathbf{P} = \tfrac{1}{2}(\mathbf{p}+\mathbf{p}') , \tag{2.26}$$

and that the initial ($\boldsymbol{\kappa}$) and final ($\boldsymbol{\kappa}'$) relative momenta are

$$\boldsymbol{\kappa} = \tfrac{1}{2}(\mathbf{K} - \mathbf{P} + \mathbf{q}), \quad \boldsymbol{\kappa}' = \tfrac{1}{2}(\mathbf{K} - \mathbf{P} - \mathbf{q}) . \tag{2.27}$$

With the above relationships the optical potential may be rewritten compactly as

$$U(\mathbf{k}',\mathbf{k};E) = \int d\mathbf{P} \sum_{\epsilon_\alpha < \epsilon_F} \varphi^\dagger_\alpha(\mathbf{p}') \hat{t}(\boldsymbol{\kappa}',\boldsymbol{\kappa};z_\alpha) \varphi_\alpha(\mathbf{p}) , \tag{2.28}$$

where

$$\hat{t}(\boldsymbol{\kappa}',\boldsymbol{\kappa};z) = \langle \boldsymbol{\kappa}' | t(z) | \boldsymbol{\kappa} \rangle , \tag{2.29}$$

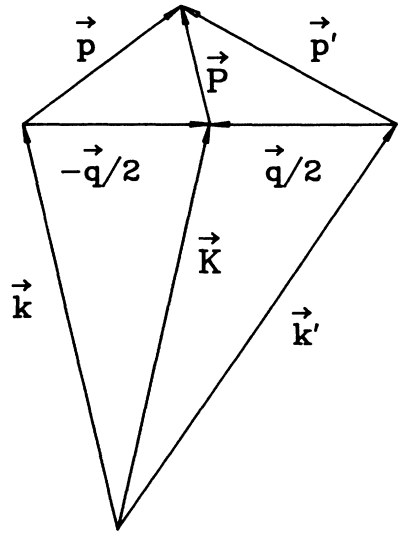

FIG. 1. Relationship between the relevant momenta in the NN collision as used in Eq. (2.28).

and the energy available in the NN system is given by

$$z_\alpha = E + \epsilon_\alpha - \frac{(\mathbf{P}+\mathbf{K})^2}{2M} . \tag{2.30}$$

By using $\mathbf{P}$ as the integration variable we are able to exploit more directly the confined Fourier components of the target bound-state wave functions.

The optical potential $U(\mathbf{k}',\mathbf{k};E)$ in Eq. (2.28) is actually an operator in the spin and isospin spaces of the projectile. For proton elastic scattering we allow for differences between proton and neutron wave functions and find

$$U(\mathbf{k}',\mathbf{k};E) = \int d\mathbf{P} \sum_{N=p,n} \sum_{\alpha_N} \varphi^\dagger_{\alpha_N}(\mathbf{p}')\hat{t}_{pN}(\boldsymbol{\kappa}',\boldsymbol{\kappa};z_{\alpha_N})\varphi_{\alpha_N}(\mathbf{p}) , \tag{2.31}$$

where the summation over α_N is restricted to occupied single-particle states of nucleon N, and $\hat{t}_{pp}$ and $\hat{t}_{pn}$ represent proton-proton and proton-neutron t matrices, respectively. To obtain a more explicit expression for the optical potential, we describe the target ground state using a shell model which allows for spin-orbit coupling. In coordinate space, the corresponding single-particle wave functions are denoted by $R_{nlj;N}(r)$, with the quantum numbers nlj the principal, orbital, and total angular momenta for the bound nucleon (N) state. Consequently, the momentum representation of the single-particle states can be expressed as

$$\varphi_{nljm_j;N}(\mathbf{p}) = (-i)^l \mathcal{R}_{nlj;N}(p)\mathcal{Y}^{m_j}_{jl}(\hat{\mathbf{p}}) , \tag{2.32}$$

where $\mathcal{R}_{nlj;N}$ represents the Fourier transform of the radial part of the single-particle wave function

$$\mathcal{R}_{nlj;N}(p) = \left[\frac{2}{\pi}\right]^{1/2} \int_0^\infty r^d dr j_l(pr) R_{nlj;N}(r) , \tag{2.33}$$

and $\mathcal{Y}^{m_j}_{jl}$ represents the coupled orbital-spin state for spin-$\frac{1}{2}$ particles defined by

$$\mathcal{Y}^{m_j}_{jl}(\hat{p}) = \sum_{m_l\mu} Y_{lm_l}(\hat{p})|\tfrac{1}{2}\mu\rangle\langle l\tfrac{1}{2}m_l\mu|jm_j\rangle . \tag{2.34}$$

Using Eq. (2.32) for the single-particle wave functions in Eq. (2.31) for the optical potential, one obtains

$$U(\mathbf{k}',\mathbf{k};E) = \int d\mathbf{P} \sum_{N=p,n} \sum_{nlj} \mathcal{R}_{nlj;N}(p')\langle \hat{t}_{pN}(\boldsymbol{\kappa}',\boldsymbol{\kappa};z_{nlj:N})\rangle_{jl} \mathcal{R}_{nlj;N}(p) , \tag{2.35}$$

where the summation on nlj runs over occupied orbitals of the target ground state, and we have defined

$$\langle \hat{t}_{pN}(\boldsymbol{\kappa}',\boldsymbol{\kappa};z)\rangle_{jl} = \sum_m \mathcal{Y}^{m\,\dagger}_{jl}(\hat{\mathbf{p}}')\hat{t}_{pN}(\boldsymbol{\kappa}',\boldsymbol{\kappa};z)\mathcal{Y}^m_{jl}(\hat{\mathbf{p}}) . \tag{2.36}$$

One of the difficulties in evaluating the full-folding potential as given by Eq. (2.35) is that of summing over the single-particle states while folding the effective interaction with the struck nucleon wave function. As noted from Eq. (2.35), this requires evaluating the effective interaction at each NN energy $z_{nlj;N}$, one for each distinct $\epsilon_{nlj;N}$ occurring in the shell-model description of the target ground state. However, at energies above 100 MeV, it is reasonable to ignore this effect by considering average energies $\langle \epsilon_N \rangle$ characteristic of protons and neutrons. This approximation simplifies significantly the coupling between the projectile and the target.

The remaining aspect to address at this point is the role of the spin-isospin degrees of freedom of the NN effective interaction in the context of the full-folding model. In spin space, the NN t matrix is an operator which may be expanded in terms of its tensorial ranks $K=0$, 1, and 2, corresponding to the central, spin-orbit and tensor components respectively. However, in the present study we consider only spin-saturated closed-shell nuclei, and in these cases contributions to the optical potential coming from the tensor component ($K=2$) of the force are expected to be neglegible.[19] Consequently, we shall omit the tensor component in the expansion of the t matrix and write

$$\hat{t}(\boldsymbol{\kappa}',\boldsymbol{\kappa};z) = \sum_{S,T} \{t^{ST;0}(\boldsymbol{\kappa}',\boldsymbol{\kappa};z) + i\mathbf{S}\cdot\hat{\boldsymbol{n}}\, t^{ST;1}(\boldsymbol{\kappa}',\boldsymbol{\kappa};z)\}P_S P_T , \tag{2.37}$$

where P_S and P_T correspond to projection operators onto NN states of total spin S and isospin T, respectively. The vectors $\mathbf{S}$ and $\hat{\mathbf{n}}$ are defined by

$$\mathbf{S} = \tfrac{1}{2}(\boldsymbol{\sigma}_0 + \boldsymbol{\sigma}_1), \quad \hat{\boldsymbol{n}} = \frac{\boldsymbol{\kappa}\times\boldsymbol{\kappa}'}{\|\boldsymbol{\kappa}\times\boldsymbol{\kappa}'\|} , \tag{2.38}$$

with $\frac{1}{2}\boldsymbol{\sigma}_0$ and $\frac{1}{2}\boldsymbol{\sigma}_1$ the spin operators for the projectile and the struck nucleon, respectively. The components $t^{ST;0}$ and $t^{ST;1}$ are of ranks 0 and 1 in spin space, respectively, and are obtained[1] from the partial-wave t-matrix elements t^{ST}_{JLL} via

$$t^{ST;0}(\boldsymbol{\kappa}',\boldsymbol{\kappa};z) = \frac{1}{4\pi}\frac{1}{2S+1}\sum_{J,L}(2J+1)t^{ST}_{JLL}(\kappa',\kappa;z)P_L(\hat{\boldsymbol{\kappa}}\cdot\hat{\boldsymbol{\kappa}}') , \tag{2.39a}$$

$$t^{ST;1}(\boldsymbol{\kappa}',\boldsymbol{\kappa};z) = \frac{1}{4\pi}\delta_{s1}\sum_{J,L}\frac{2J+1}{2L(L+1)}[\mathbf{L}\cdot\mathbf{S}]_{JL} \times t^{ST}_{JLL}(\kappa',\kappa;z)P^1_L(\hat{\boldsymbol{\kappa}}\cdot\hat{\boldsymbol{\kappa}}') , \tag{2.39b}$$

with the definition

$$[\mathbf{L}\cdot\mathbf{S}]_{JL} = \tfrac{1}{2}\{J(J+1) - L(L+1) - S(S+1)\} . \tag{2.40}$$

The pp and pn components of the force required in Eq. (2.35) are simply related to states of total isospin $T=0$ and 1. If we define

$$\hat{t} \equiv \sum_T \hat{t}^{\,T} P_T \ , \tag{2.41}$$

then

$$\hat{t}_{pp} = \hat{t}^{\,T=1} \ , \tag{2.42a}$$

$$\hat{t}_{pn} = \tfrac{1}{2}(\hat{t}^{\,T=0} + \hat{t}^{\,T=1}) \ . \tag{2.42b}$$

Furthermore, in the spin space of the struck nucleon, each of the pN components can be reduced to a sum of scalar and vector terms. Therefore, for calculating $\langle \hat{t} \rangle_{jl}$ one needs to evaluate the elements $\langle I_1 \rangle_{jl}$ and $\langle \sigma_1 \rangle_{jl}$, with I_1 and $\frac{1}{2}\sigma_1$ the identity and spin, respectively. The use of definition (2.36) for $\langle \ \rangle_{jl}$ and standard angular-momentum identities yield

$$\langle I_1 \rangle_{jl} = \frac{1}{4\pi}(2j+1) P_l(\hat{\mathbf{p}} \cdot \hat{\mathbf{p}}') \tag{2.43}$$

$$\langle \sigma_1 \rangle_{jl} = \frac{1}{4\pi} i \hat{\mathbf{n}} \frac{2j+1}{2l(l+1)} [\mathbf{l} \cdot \sigma_1]_{jl} P_l^1(\hat{\mathbf{p}} \cdot \hat{\mathbf{p}}') \ , \tag{2.44}$$

where

$$[\mathbf{l} \cdot \sigma_1]_{jl} = j(j+1) - l(l+1) - \tfrac{3}{4} \ , \tag{2.45a}$$

$$\hat{\mathbf{n}} = \frac{\mathbf{p}' \times \mathbf{p}}{\|\mathbf{p}' \times \mathbf{p}\|} \ . \tag{2.45b}$$

The role of the $\langle \ \rangle_{jl}$ matrix elements is analyzed in the context of Eq. (2.35) for the full-folding optical potential. For example, when those terms of $\langle \hat{t} \rangle_{jl}$ proportional to $\langle \sigma_1 \rangle_{jl}$ are multiplied by the wave functions and j is summed over for a fixed l ($l \neq 0$), the integrand in Eq. (2.35) becomes proportional to

$$2l(l+1)\{\mathcal{R}_+(p')\mathcal{R}_+(p) - \mathcal{R}_-(p')\mathcal{R}_-(p)\} \ ,$$

where $\mathcal{R}_\pm$ is a shorthand for $\mathcal{R}_{nll\pm 1/2}$. Contributions of this type have been neglected in the present calculations. The implicit assumption is that of a small difference between the wave functions $\mathcal{R}_\pm$ in the region where the dominant contributions to the full-folding integral occur. This approximation is expected to be quite reasonable at intermediate energy for the nuclei considered here.

With the above consideration, the optical potential is determined by those components of the t matrix proportional to I_1 and is given by

$$U(\mathbf{k}',\mathbf{k};E) = \int d\mathbf{P} \sum_{N=p,n} \sum_{nlj} \frac{(2j+1)}{4\pi} \mathcal{R}_{nlj;N}(p') \mathcal{R}_{nlj;N}(p) P_l(\hat{\mathbf{p}} \cdot \hat{\mathbf{p}}') \{ t_{pN}^C(\boldsymbol{\kappa}',\boldsymbol{\kappa};z_N) + i\tfrac{1}{2}\sigma_0 \cdot \hat{\mathbf{n}} t_{pN}^{LS}(\boldsymbol{\kappa}',\boldsymbol{\kappa};z_N) \} \ , \tag{2.46}$$

with t_{pN}^C and t_{pN}^{LS} specified in Appendix A.

Calculations of the full-folding optical potential as given by Eq. (2.46) were performed for proton elastic scattering on ^{16}O and ^{40}Ca at energies between 135 and 500 MeV. No approximations were made to treat either the off-shell t matrix or the single-particle wave functions. Some of the aspects of calculating the optical potential and applying it to proton elastic scattering which require special consideration are outlined in Sec. III.

III. CALCULATIONS

A. The full-folding integral

The calculation of each matrix element of the full-folding optical potential expressed by Eq. (2.46) requires an explicit integration over the momentum $\mathbf{P}$ [$\mathbf{P} = \frac{1}{2}(\mathbf{p}+\mathbf{p}')$]. In principle, the variation of $\mathbf{P}$ is unrestricted. However, the localized momentum distribution of the bound target nucleons justifies limiting the integration over P to a relatively small volume. This was implemented by cutting off the high Fourier components of the ground-state wave functions at some momentum P_c, typically of the order of ~ 3 fm^{-1}. The cutoff momentum defines an overlapping volume formed by the wave functions of the struck nucleon before and after the collision. The situation is illustrated in Fig. 2, where the origins of the wave functions are placed at $\mathbf{k}$ and $\mathbf{k}'$, respectively. The separation between these two origins is given by $\mathbf{q}$, the momentum transferred to the struck nucleon. The overlapping volume is defined by the conditions $p < P_c$ and $p' < P_c$, and represents the region responsible for the non-negligible contributions to the optical potential. As observed from Fig. 2, the overlap diminishes as the momentum transfer increases. The use of the above restrictions dramatically reduces the time required for calculating the optical-potential matrix elements. Our criteria for determining an appropriate value for P_c for the

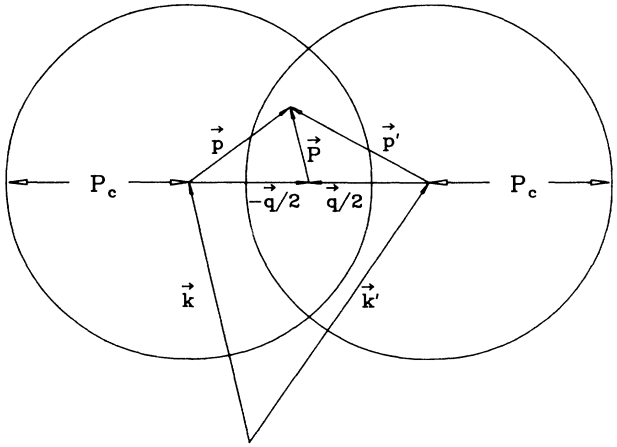

FIG. 2. Diagram of the overlap between the struck nucleon wave functions before and after the collision. P_c represents the cutoff momentum.

calculation of the optical potential was based on studies of convergence of the calculated scattering observables for $0 \leq q \leq 3.5$ fm^{-1}.

One of the distinctive features of the full-folding optical potential is that it probes the effective interaction off the energy shell over a wide range of energy and relative momenta. To implement this feature we have evaluated the t matrix over a broad region in momentum space as well as over a wide range of energies in the NN center-of-mass (c.m.) system. The effective interaction used throughout was the free t matrix from the Paris potential,[20] calculated fully off shell up to energies of 500 MeV in the NN c.m. system, and out to relative momenta of the order of ~ 10 fm^{-1}. To verify convergence of the calculated potentials, different sets of t matrices were used at alternative mesh points in the relative momenta and NN c.m. energies. The t matrices were generated for all allowed NN states through $J=8$. The required antisymmetric structure was maintained by restricting the t matrix to those NN states allowed by the Pauli principle. In this way the knockon exchange term in the NN scattering was accounted for naturally without having to separate the interaction into direct and exchange components.

The off-shell t matrix for the Paris potential was calculated using two distinct methods to rule out the possibility of introducing spurious off-shell matrix elements in the calculations. One of the methods consists of solving a non-homogeneous Schrödinger equation with a source term to allow for off-shell NN scattered waves, as proposed by Van Leewen and Reiner,[21] implemented to include momentum-dependent potentials such as the Paris potential.[22] The other method is a continued-fraction scheme[23] implemented for solving integral equations of the Lippmann- Schwinger form. The two calculated sets of t matrices were then used to calculate the full-folding optical potential. When applications to proton elastic scattering were made, agreement within 3% was observed for the calculated scattering observables for $q \lesssim 3.5$ fm^{-1}.

B. Treatment of the Coulomb potential

The calculation of the optical potential was performed in momentum space. This makes it appealing, therefore, to calculate the scattering observables in the same representation. However, when studying proton scattering, the long range of the Coulomb potential leads to a $\sim 1/q^2$ singularity in momentum space which is very difficult to handle accurately. Although approximations have been suggested for treating this problem,[24,25] we have found that the scattering observables, especially the spin observables, are very sensitive to the degree of accuracy of the method. Since the objective of this work is to study the optical model in a scheme sufficiently accurate for comparing measured and calculated observables, it was essential to establish the reliability of the calculated scattering observables in the presence of Coulomb potentials.[9] This was done by performing the scattering calculations in momentum and coordinate representations, using different approaches to solve the scattering problem. Results reported in this work for the calculated scattering observables are shown in those ranges of momentum transfer where we found systematic agreement between results obtained from the two approaches.

The momentum-space calculations were performed using the Lippmann-Schwinger integral equation for proton elastic scattering. In this case we applied the method proposed by Vincent and Phatak[24] (VP) for treating the nuclear coupling in the presence of a Coulomb potential. The method consists of calculating the phase shifts corresponding to an alternative short-range problem, where the asymptotic $\sim Ze^2/r$ Coulomb potential is cut off at some radius R_c. The resulting phase shifts are then used in the VP transformation, which relates the phase shifts associated with the actual scattering problem to those obtained by setting the Coulomb potential to zero for $r > R_c$. In the momentum-space calculations, the inner part of the Coulomb potential is given by

$$\tilde{V}_{\rm Coul}(q) = \frac{Ze^2}{2\pi^2 q^2}[\tilde{\rho}_{\rm ch}(q) - \cos(qR_c)] \ , \tag{3.1}$$

where $\tilde{\rho}_{\rm ch}(q)$ is the Fourier transform of the charge density.

One of the important requirements for a consistent implementation of the VP method is that of choosing R_c, the cutoff radius, large enough to ensure convergence of the calculated phase shifts for the actual problem. In practice, this condition is met at distances of the order of 10 to 15 fm, the usual matching radii for scattering calculations of nucleons in the presence of local nuclear potentials. Consequently, one has to proceed carefully in extracting the multipoles of $V_{\rm Coul}$ in (3.1) due to the rapidly oscillating term $\cos(qR_c)$. In this respect, we have implemented very accurate multipole expansions for the modified Coulomb potential,[26] which in the case of simple charge distributions result in analytic expressions.

Recent reports[25] have noted the difficulties of implementing the VP method accurately for proton scattering at intermediate energies. In light of this, independent calculations of the scattering observables were performed in coordinate space, where reliable methods for treating the Coulomb potential are well established. In this case we solved the Schrödinger equation in the form of an integrodifferential equation, as required when explicit nonlocal potentials are treated. One of the advantages of this approach is its simplicity; another is that of obtaining the scattering wave functions which can be useful for other applications. However, this approach is computationally more intense since it requires calculating and storing Bessel functions for many arguments and partial waves as well as transforming the momentum-space potential to a coordinate representation.

In order to illustrate the level of agreement between the momentum and coordinate representation calculations, we show in Fig. 3 the calculated differential cross section ($d\sigma/d\Omega$), analyzing power (A_y), and spin-rotation parameter (Q) obtained from each approach for elastic scattering of protons on ^{40}Ca at 400 MeV as functions of q, the momentum transfer. Calculations at other energies and for other targets show similar agreement. We find very close agreement for each observable up to

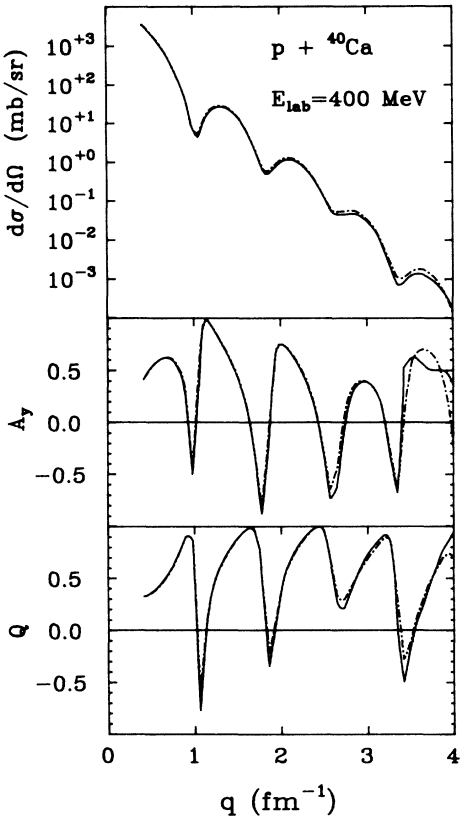

FIG. 3. Calculated scattering observables for $p+^{40}$Ca at 400 MeV using momentum-space (solid curve) and coordinate-space (dashed-dotted curve) procedures.

momentum transfers of ~ 2.5 fm^{-1}, beyond which a slight deviation between the two calculations is noticed. Between 2.5 and 3.5 fm^{-1} the agreement is still reasonable, but beyond 3.5 fm^{-1} differences are acute. Since the differences up to $q \sim 3.5$ fm^{-1} are still acceptable and the dominant qualitative features of the scattering observables consistently reproduced, we set 3.5 fm^{-1} as the upper limit in q for which the calculated scattering observables are reliable. The extension of this range to larger q would require further refinements.

C. Sensitivity to the mixed density

For the calculation of the optical potential it is desirable to have a realistic set of bound-state wave functions in the sense they give an optimum account of the physical properties of the target ground state. Although electron scattering provides extremely important constraints on the ground-state charge density, it does not determine the *mixed* density required by the full-folding model. In light of this and other uncertainties in the description of the ground state, it is useful to have an estimate of the degree of sensitivity of the calculated scattering observables to the single-particle model used in the calculation of the optical potential. In order to illustrate this sensitivity, we have calculated the optical potential for $p+^{40}$Ca scattering at 200 MeV using two different shell models for the target ground state. One of these models was the Woods-Saxon (WS) model with parameters adjusted to reproduce the root-mean-square (rms) charge radius; the other was a standard harmonic oscillator (HO) model with a single oscillator parameter ($\alpha = 0.5136$ fm^{-1}) consistent with the rms radius of the WS wave functions. To allow a more transparent interpretation of the results we have taken, for this comparison, the neutron wave functions to be the same as those for the protons. The calculated cross sections, analyzing powers, and spin-rotation parameters are shown in Fig. 4 as functions of the momentum transfer. Figure 4 also shows the squared Fourier transforms of the nuclear densities. The solid and dotted lines in Fig. 4 represent the WS and HO models, respectively. From Fig. 4 it is noted that at $q \lesssim 1$ fm^{-1} both models yield very similar $\rho(q)^2$. Differences begin to appear for $q \gtrsim 1$ fm^{-1}, where an indication of ρ_{HO} being less negative than ρ_{WS} is observed. This trend is maintained up to $q \approx 2$ fm^{-1}, above which the differences are noticeable even qualitatively. When com-

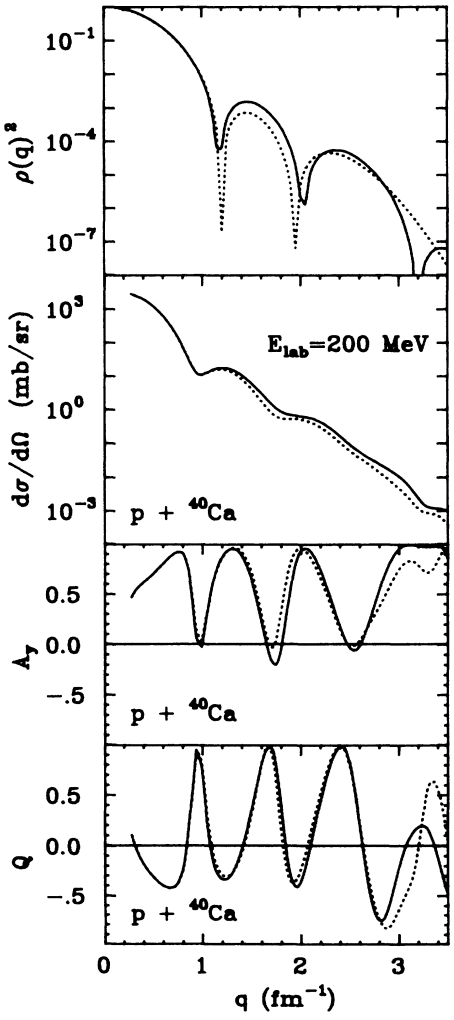

FIG. 4. Squared Fourier transform of nuclear densities and corresponding scattering observables for $p+^{40}$Ca at 200 MeV calculated in the full-folding model. Solid and dotted curves are used to represent the WS and HO results, respectively.

paring the calculated scattering observables we see that both models yield very similar results up to $q \approx 1.5$ fm^{-1}. Beyond this momentum the differences are characterized by a slight shift forward of each observable calculated from the HO model with respect to the WS model, a feature also present in the ρ^2 plot.

IV. RESULTS AND ANALYSIS

Calculations of the full-folding optical potential were made for proton scattering on ^{16}O and ^{40}Ca at energies between 135 and 500 MeV. The calculated scattering observables are compared with those obtained using the standard on-shell $t\rho$ model of the optical potential and with the data. When comparing the two types of calculations we should keep in mind that the on-shell $t\rho$ model constitutes an approximation to the full-folding model. The major differences between *calculated* results obtained using the two approaches are an indication of the importance of off-shell effects in the theory. As mentioned earlier, explicit medium corrections have been neglected.

The on-shell $t\rho$ potential was calculated by multiplying the Fourier transform of the nuclear densities by the free t matrix evaluated on shell at a NN energy z_B given by the Breit invariant mass S_B.[4] Allowing for differences between the proton and neutron densities, the optical potential takes the form

$$U(q;E)=\tilde{\rho}_P(q)\hat{t}_{pp}[q;z_B(q)]+\tilde{\rho}_n(q)\hat{t}_{pn}[q;z_B(q)] , \quad (4.1)$$

where

$$z_B(q)=\sqrt{S_B(q)}-2m , \quad (4.2a)$$

$$S_B(q)=[(m^2+k_0^2)^{1/2}+(m^2+\tfrac{1}{4}q^2)^{1/2}]^2-(k_0^2-\tfrac{1}{4}q^2) , \quad (4.2b)$$

with k_0 the projectile incident momentum in the nucleon-nucleus center of mass. At a given incident energy, the resulting potential is a function of only the momentum transfer, and therefore has an explicit local structure in coordinate space.

The full-folding potentials were calculated using the procedures outlined in Sec. III. The single-particle model used in this analysis was a WS model fit to the rms radius of the point-proton density determined from electron scattering and to experimental single-particle energies. In the case of ^{16}O, the resulting set of wave functions gave a point rms radius of 2.62 fm for protons and 2.58 fm for neutrons, with average binding energies of -23.8 and -27.3 MeV, respectively. In the case of ^{40}Ca, the WS model gave a point rms radius of 3.37 fm for protons and 3.30 fm for neutrons; the corresponding average binding energies were -24.0 and -31.4 MeV, respectively. The same wave functions were used for the full-folding and $t\rho$ calculations. For each nucleus the calculated and measured charge form factors are in reasonable agreement out to $q \sim 2.5$–3.0 fm^{-1}.

Although the use of the Möller factor[11] for transforming the t matrix from the NN c.m. to the nucleon-nucleus c.m. frame is not consistent within a purely nonrelativistic formulation of the full-folding model, we have included this term in the present calculations in order to account for relativistic effects of a kinematical origin. However, we have found that the importance of corrections of this type within the full-folding model are relatively small, leading to only slight changes in the cross section and much smaller changes in the spin observables.

In light of the limitations of the NN potential model above $\sim$400 MeV noted earlier, comparisons between measured and calculated results at 500 MeV presented below cannot be regarded as tests of the full-folding model or of any approximation to it. Nevertheless, at this higher energy the Paris potential should be sufficiently realistic for obtaining meaningful comparisons between different theoretical approaches.

A. Results for $p + ^{16}$O elastic scattering

In Fig. 5 we present measured and calculated observables for $p + ^{16}$O elastic scattering at 135, 200, and 500 MeV as a function of the momentum transfer. The data were taken from Refs. 27, 28, and 29, respectively. Results obtained from the full-folding and on-shell $t\rho$ calculations are represented with solid and dotted curves respectively. The most striking features we observe from Fig. 5 are the significant differences between the two theoretical approaches, with the full-folding model providing a clearly superior description of the data at 135 and 200 MeV. The largest differences between the two models occur in the cross sections and analyzing powers at 135 and 200 MeV and at momentum transfers below ~ 2.2 fm^{-1}. At these energies, for example, the $t\rho$ model overestimates the cross section significantly at forward scattering angles, whereas the full-folding model follows the data more closely. In addition, at each energy the $t\rho$ model predicts a diffractive minimum in the cross section near $q \approx 1$ fm^{-1} which the data do not exhibit. Another feature of the full-folding model is its ability to give a reasonable account of the measured A_y at 135 MeV, and A_y and Q at 200 MeV. The locations of the maxima and minima, as well as their corresponding values, are described reasonably well by the full-folding model. In contrast, the on-shell $t\rho$ model fails to reproduce, even qualitatively, the general features of the measured analyzing power. These differences illustrate the importance of off-shell effects in the scattering at forward angles. This is consistent with the fact that for small momentum transfer, the overlap between the wave functions of the struck nucleon before and after the collision is maximized. As a result, a maximum variation of **P** is allowed (see Fig. 2) leading to a broad off-shell sampling of the t matrix [see Eqs. (2.27) and (2.30)].

At 500 MeV proton energy, *calculated* results from the full-folding and $t\rho$ models are in comparable agreement with the data, although the full-folding model still provides a superior description of the cross section and the analyzing power data at small momentum transfer. However, at this energy the spin-rotation parameter predicted by the full-folding model possesses too little structure, whereas the $t\rho$ model follows the general pattern of maxima-minima given by the data. This deterioration of

the agreement between the calculated observables and the data will be addressed later.

B. Results for $p + {}^{40}Ca$ elastic scattering

In Fig. 6 the measured and calculated observables for $p + {}^{40}Ca$ scattering are shown as a function of the momentum transfer q. Results obtained from the full-folding calculations and the on-shell $t\rho$ approximation are represented by the solid and dotted curves, respectively. The sequence of energies considered in Fig. 6 are 200, 300, 400, and 500 MeV. The data at 200 MeV were taken from Ref. 28. The cross section and analyzing power data at 300, 400, and 500 MeV were taken from Ref. 30. In the case of the spin-rotation parameter data shown at 300 MeV, we used data taken at 320 MeV from Ref. 29 and plotted them as function of q. The Q data at 500 MeV were taken from Ref. 31.

As in the case of $p + {}^{16}O$ elastic scattering, the full-folding model provides a reasonable description of the measured elastic scattering observables, being superior to the on-shell $t\rho$ approximation results at energies near and below ~ 400 MeV. At 200 MeV, for example, the agreement between the full-folding model results with the data is quite reasonable up to $q \sim 2.5$ fm^{-1}. At this energy the on-shell $t\rho$ model overestimates the cross section at forward angles and yields a diffractive minimum near $q \approx 1$ fm^{-1} which is much more pronounced than is observed. Moreover, the full-folding model provides a very good account of the maxima-minima pattern of the measured analyzing power, whereas the on-shell $t\rho$ model predicts minima which are much too shallow with maxima being slightly shifted with respect to the data. At 300 and 400 MeV proton scattering, the description of the data by the full-folding model is very reasonable in the range of q between 1 and 2.5 fm.$^{-1}$ At these energies, both the cross section and the analyzing power are very well described by the full-folding model, following closely the maxima-minima pattern of the data. For $q \lesssim 1$ fm^{-1}, however, both models overestimate the first maximum in A_y, although the $t\rho$ model does so more strongly. It is interesting to notice that at energies above 200 MeV, the $t\rho$ mod-

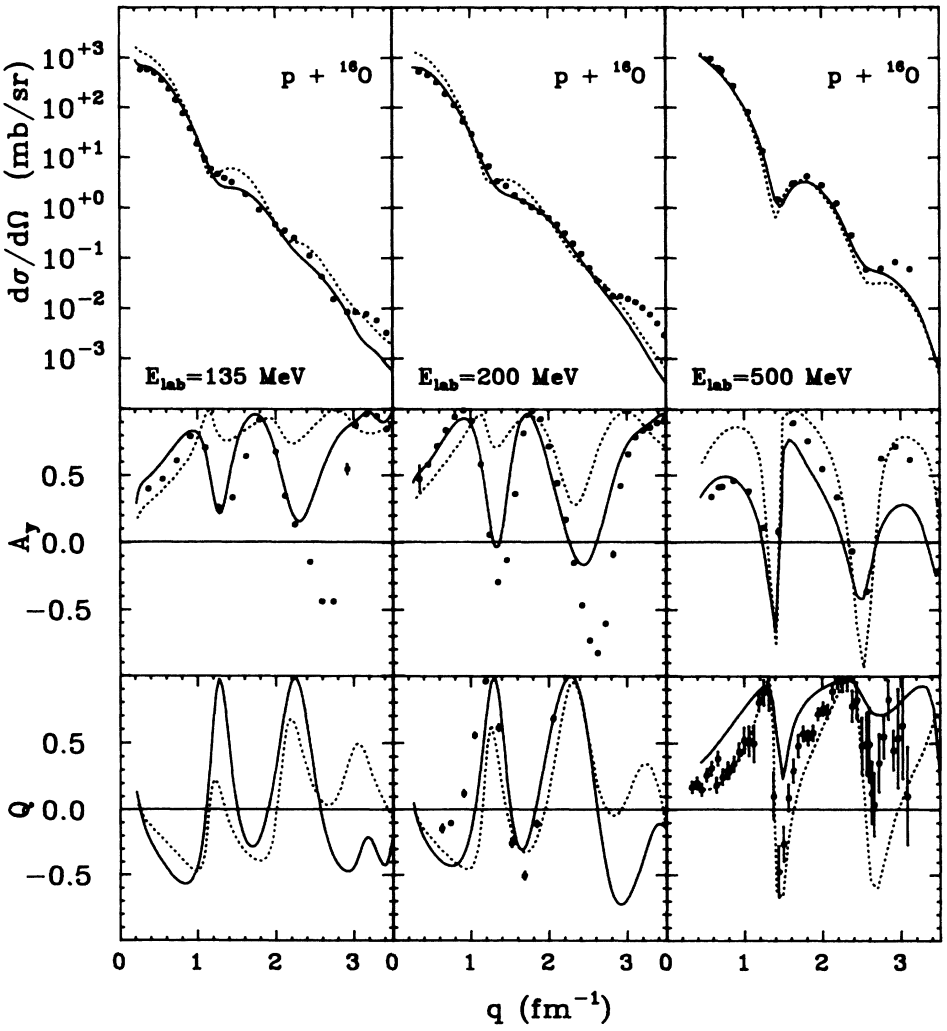

FIG. 5. Calculated and measured elastic scattering observables for $p + {}^{16}O$ at 135, 200, and 300 MeV. The data are from Refs. 26, 27, and 28, respectively. Solid curves represent full-folding results; dotted curves represent on-shell $t\rho$ results.

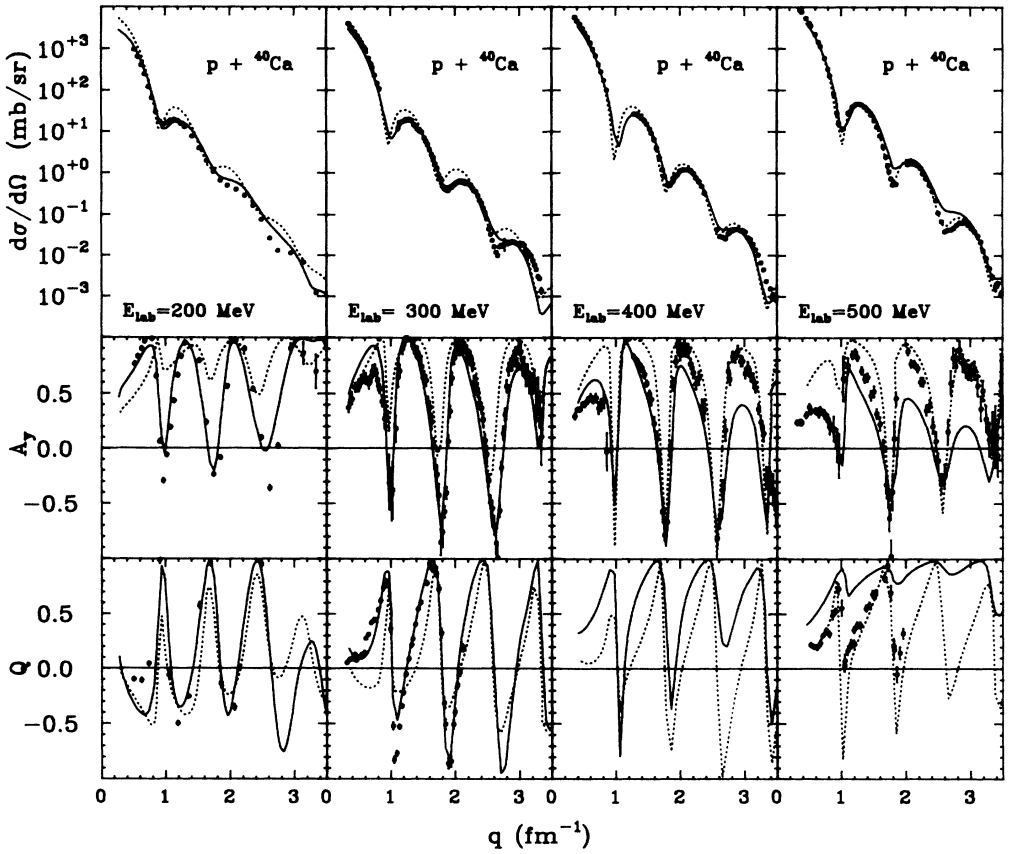

FIG. 6. Calculated and measured elastic scattering observables for $p+^{40}$Ca at 200, 300, 400, and 500 MeV. The data are from Refs. 27–30 (see text). Solid curves represent full-folding results; dotted curves represent on-shell $t\rho$ results. *The Q data shown at 300 MeV correspond to measurements made at 320 MeV.*

el results for the cross section are systematically shifted forward relative to the data, a deficiency which is not present in the full-folding model results.

As noted for $p+^{16}$O scattering at 500 MeV, the 500 MeV results presented in Fig. 6 show a considerable deterioration of the agreement between the measured and calculated observables. These differences are more pronounced than those observed at lower energies and are more noticeable in the case of the spin observables. Results at 400 MeV for $p+^{40}$Ca scattering show that the deterioration in A_y beyond 1 fm^{-1} is confined primarily to $q \gtrsim 2.5$ fm^{-1}, whereas at 500 MeV the lack of structure in the calculated $A_y(Q)$ occurs for essentially all q greater than 1 (0) fm^{-1}. Apart from the deterioration between full-folding results and the data, we also note significant differences between the on-shell $t\rho$ and the full-folding calculations. This result demonstrates the important role of off-shell degrees of freedom in nucleon-nucleus scattering for projectile energies as high as 500 MeV.

C. The off-shell $t\rho$ approximation

To illustrate the role of off-energy-shell effects *within* the full-folding model, we have performed calculations using an off-shell $t\rho$ approximation and have compared the results with those obtained from the full-folding model. Results from the on-shell $t\rho$ approximation were also included for comparison.

The off-shell $t\rho$ approximation at intermediate energies was obtained by neglecting the variation of the t matrix with respect to $\mathbf{P}$ in Eq. (2.28) in the region where the product of the wave functions peaks ($\mathbf{P}\approx 0$). Therefore, to lowest order in a series expansion about $\mathbf{P}=0$, we can approximate the t matrix by its value at $\mathbf{P}=0$ and then integrate the remaining terms involving only the wave functions. This leads to a factorized $t\rho$ structure for the optical potential which reads

$$U(\mathbf{k}',\mathbf{k};E)\approx U_0(\mathbf{k}',\mathbf{k};E)=\sum_N \tilde{\rho}_N(q)\hat{t}_{pN}(\boldsymbol{\kappa}',\boldsymbol{\kappa};z_N)\Big|_{\mathbf{P}=0}, \tag{4.3}$$

where the variables $\mathbf{k}'$ $\mathbf{k}$, and z_N have been defined in Eqs. (2.27) and (2.30). The off-shell $t\rho$ approximation given by Eq. (4.3) is similar to those recently applied[25,32] for the purpose of studying off-shell effects using other interactions. The difference is, however, the energy prescription for the t matrix. In the application of Ref. 32 the energy z_N was fixed to a value corresponding to free NN scattering at the beam energy. In the present application we follow the energy prescription used for the full-folding model, that is, the one given by Eq. (2.30) evaluated at $\mathbf{P}=0$

and with ϵ_α replaced by an average value as described previously. In this way we shall be able to more reliably identify those unique features of the full-folding model.

In Fig. 7 we show the calculated observables for $p+{}^{16}$O scattering at 135 and 200 MeV and in Fig. 8 those corresponding to $p+{}^{40}$Ca scattering at 200 300 MeV. The solid, dashed, and dotted curves denote the full-folding, off-shell $t\rho$, and on-shell $t\rho$ results, respectively. The most pronounced differences between the off-shell $t\rho$ and the full-folding results occur at the lower energies. As the energy increases, the full-folding and off-shell $t\rho$ results are in closer agreement. Although this feature suggests that the off-shell $t\rho$ approach could be a suitable approximation to the full-folding model at high energies, its validity needs to be assessed in the context of a broader class of NN effective interactions. Very recent calculations[33] using the Bonn potential, in which further simplifying assumptions are made to treat the t-matrix off shell within the full-folding framework, yield scattering observables which are very similar to those obtained in the off-shell $t\rho$ approximation for $p+{}^{16}$O scattering at 200 and 500 MeV.

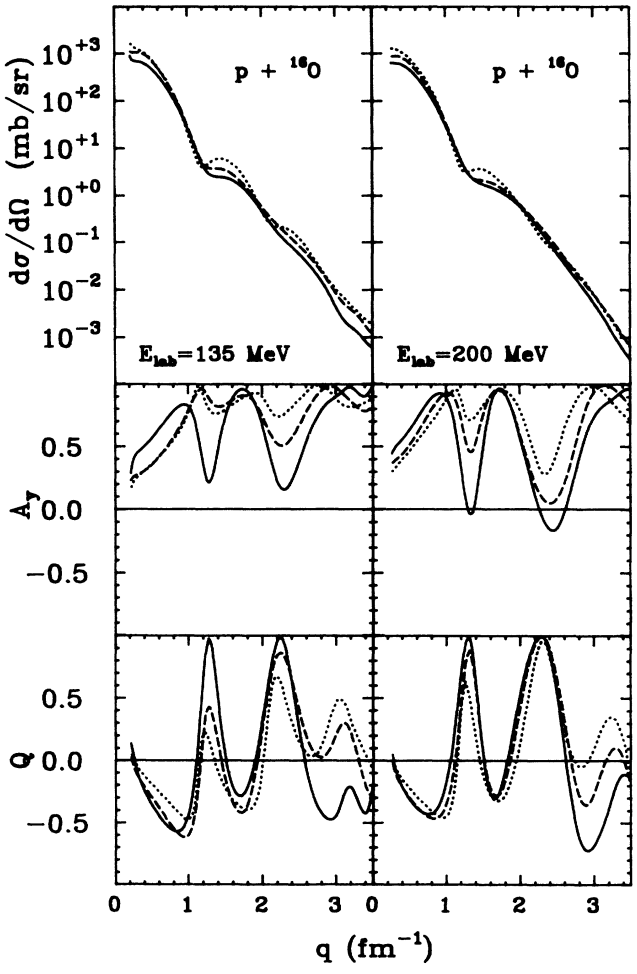

FIG. 7. Calculated elastic scattering observables for $p+{}^{16}$O at 135 and 200 MeV. Solid, dashed, and dotted curves represent full-folding, off-shell, and on-shell results, respectively.

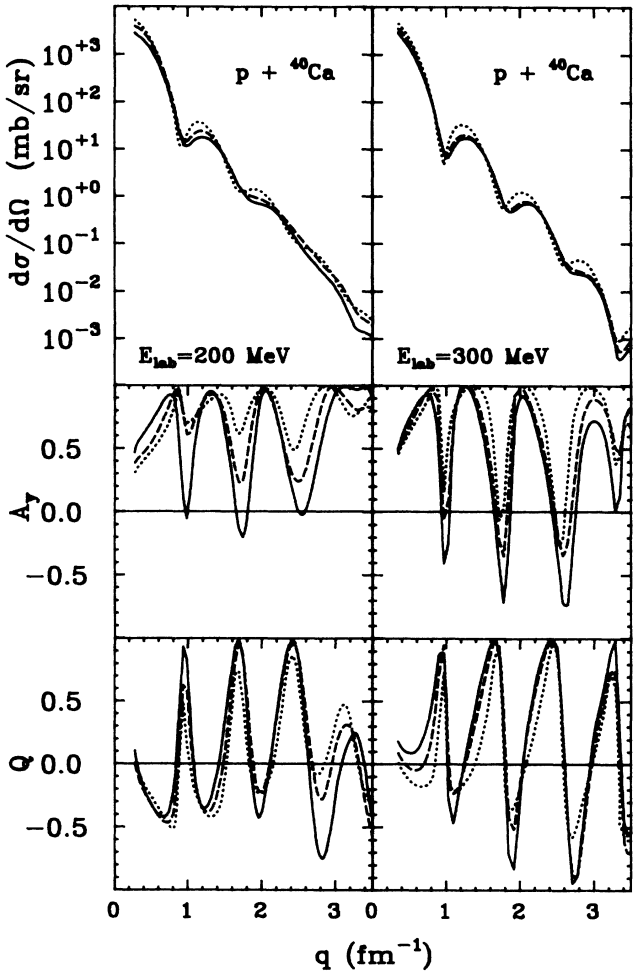

FIG. 8. Calculated elastic scattering observables for $p+{}^{40}$Ca at 200 and 300 MeV. Solid, dashed, and dotted curves represent full-folding, off-shell, and on-shell results, respectively.

Another feature we observe from Figs. 7 and 8 is that at the lower energies the description of the scattering observables obtained from the two $t\rho$ approximations are very similar, but differ substantially from those obtained in the full-folding approach. These results demonstrate that neither factorized $t\rho$ approximation considered here accounts properly for all off-shell effects included in the full-folding model.

V. SUMMARY AND CONCLUSIONS

We have calculated nonrelativistic full-folding optical model potentials and applications have been made to proton elastic scattering from ^{16}O and ^{40}Ca at energies between 135 and 500 MeV. The full-folding calculations were performed using the free NN t matrix based on the Paris potential. The target mixed density was constructed using wave functions from a Woods-Saxon single-particle model fit to electron-scattering data and to single-particle energies. Off-shell effects, energy dependence, and knockon exchange terms of the t matrix as well as the ground-state mixed density were treated ex-

plicitly. No explicit medium corrections were included. Scattering observables obtained using the full-folding model were compared with those measured as well as those calculated from on- and off-shell $t\rho$ approximations to it. Striking differences between the full-folding and the on-shell $t\rho$ results for the scattering observables were found. With the exception of the 500 MeV results, the full-folding model provides a description of the scattering data which is superior to that obtained using either the on-shell $t\rho$ or off-shell $t\rho$ approximation. This result demonstrates the importance of treating off-shell effects of the *NN* effective interaction explicitly as prescribed by the full-folding model.

The difficulties in satisfactorily describing the 500 MeV data, especially spin observables for $p+{}^{40}$Ca elastic scattering, are common to all three theoretical approaches considered in the present analysis. However, a conclusive evaluation of the nonrelativistic full-folding model at energies above $\sim$400 MeV requires a more reliable description of the *NN* force at shorter distances *and* at higher energies, provided an *NN* potential model is theoretically justifiable under these conditions. In the case of the Paris potential, which was constructed to describe *NN* scattering at nucleon energies up to 330 MeV, the description of the *NN* force at internucleon distances smaller than 0.8 fm is purely phenomenological[20] and this parametrization of the force may not account adequately for the subnucleonic degrees of freedom. The short-range parts of the *NN* interaction are critical for determining the off-shell behavior of the effective interaction at large relative momenta. Therefore, our present limited knowledge of the *NN* force at short distances and over a limited range of energies, combined with the sensitivity of the full-folding model to the off-shell behavior of the effective interaction, precludes an absolute evaluation of the nonrelativistic full-folding model. In a broader perspective, given the sensitivity of nucleon-nucleus scattering to the off-shell behavior of the *NN* effective force, nucleon-nucleus scattering, interpreted within the full-folding model framework could provide constraints additional to those imposed by *NN* phenomenology for discriminating between alternative models of the *NN* interaction.

Although relativistic effects other than those of purely kinematical origin are expected to be present in the *NN* interaction and have not been treated explicitly, they are of course included implicitly, to some extent, in the parametrization of the *NN* potential which is used in the Schrödinger equation to describe *NN* scattering. This is the case of the Paris potential, where we have emphasized a consistent connection between the framework for describing the *NN* interaction and the formulation of the nonrelativistic full-folding model for the optical potential.

Beyond the existing limitations for describing the *NN* interaction at small distances, significant differences were noted between the *calculated* nucleon-nucleus scattering observables at 500 MeV using the full-folding model and the on-shell $t\rho$ approximation, with no indication of convergence between the two approaches with increasing energy. This demonstrates that, for the Paris potential, the on-shell $t\rho$ approach is an inadequate approximation to the full-folding model. Furthermore, this is an indication of the importance of off-shell effects in the theory and shows that *NN* phenomenology alone is insufficient for describing correctly more complex processes such as nucleon-nucleus scattering.

From the present study we conclude that off-shell effects of the *NN* effective interaction are important in the theory of nucleon-nucleus scattering. Moreover, the level of agreement between measured and calculated nucleon-nucleus scattering observables is improved substantially when these off-shell effects are treated accurately in the full-folding model of the optical potential. Features which have traditionally been difficult to explain using standard nonrelativistic approaches to nucleon-nucleus scattering at intermediate energies, such as spin observable data, are largely accounted for by the full-folding model when off-shell degrees of freedom are treated accurately. These results indicate that the first-order nonrelativistic theory describes the essential physics of this many-body problem. Furthermore, the full-folding model provides a much better first-order approximation to the nucleon-nucleus optical potential down to much lower incident energies than do its $t\rho$ variants. On the other hand, medium effects, in general, and Pauli blocking corrections, in particular, have been found to be important in earlier calculations using averaged density-dependent local forces. The role of such effects needs to be reexamined within the full-folding framework. Work in this direction is in progress.

ACKNOWLEDGMENTS

We appreciate the generous amount of computer time provided by the Department of Physics and Astronomy and the University Computing and Networking Services at the University of Georgia. This work was supported in part by the National Science Foundation under Grants Nos. PHY-8607684 and PHY-8903856. F.A.B. acknowledges partial support from the Fondo Nacional de Desarrollo Científico y Tecnológico, Chile (FONDECYT), Grant 1212-88.

APPENDIX A

To obtain expressions for t_{pN}^{C} and t_{pN}^{LS} in Eq. (2.46) we use the following representation for the spin projection operator,

$$P_S=\begin{cases}\frac{1}{4}(1-\boldsymbol{\sigma}_0\cdot\boldsymbol{\sigma}_1) & \text{for } S=0\\ \frac{1}{4}(3+\boldsymbol{\sigma}_0\cdot\boldsymbol{\sigma}_1) & \text{for } S=1\end{cases}, \tag{A1}$$

which satisfies the property

$$P_S\mathbf{S}\cdot\hat{\boldsymbol{n}}=\delta_{S1}\mathbf{S}\cdot\hat{\boldsymbol{n}}\ . \tag{A2}$$

Combining Eqs. (2.37), (2.41), (A1), and (A2) one obtains

$$\hat{t}^{\,T}=\tfrac{1}{4}(t^{0T;0}+3t^{1T;0})-\tfrac{1}{4}(t^{0T;0}-t^{1T;0})\boldsymbol{\sigma}_0\cdot\boldsymbol{\sigma}_1 +i\tfrac{1}{2}(\boldsymbol{\sigma}_0+\boldsymbol{\sigma}_1)\cdot\hat{\boldsymbol{n}}t^{1T;1}\ . \tag{A3}$$

Finally, retaining only those terms of $\hat{t}^{\,T}$ independent of the spin of the struck nucleon (σ_1) and using (2.42a) and (2.42b) for t_{pp} and t_{pn}, we obtain

$$t_{pp}^{C}=\tfrac{1}{4}(t^{01;0}+3t^{11;0}) , \tag{A4}$$

$$t_{pn}^{C}=\tfrac{1}{8}(t^{00;0}+3t^{10;0}+t^{01;0}+3t^{11;0}) , \tag{A5}$$

$$t_{pp}^{LS}=t^{11;1} , \tag{A6}$$

$$t_{pn}^{LS}=\tfrac{1}{2}(t^{10;1}+t^{11;1}) . \tag{A7}$$

[1]F. A. Brieva and J. R. Rook, Nucl. Phys. **A291**, 317 (1977); **A297**, 206 (1978); **A307**, 493 (1978).

[2]H. V. von Geramb, in *The Interaction Between Medium Energy Nucleons in Nuclei,* edited by H. O. Meyer (AIP, New York, 1983).

[3]L. Rikus and H. V. von Geramb, Nucl. Phys. **A426**, 496 (1984).

[4]L. Ray and G. W. Hoffmann, Phys. Rev. C **31**, 538 (1985).

[5]S. Mellema, R. W. Finlay, F. S. Dietrich, and F. Petrovich, Phys. Rev. C **28**, 2267 (1983).

[6]D. P. Murdock and C. J. Horowitz, Phys. Rev. C **35**, 1442 (1987).

[7]N. Ottenstein, S. J. Wallace, and J. A. Tjon, Phys. Rev. C **38**, 2272 (1988); **38**, 2289 (1988).

[8]B. C. Clark, S. Hama, R. L. Mercer, L. Ray, G. W. Hoffmann, and B. D. Serot, Phys. Rev. C **28**, 1421 (1983).

[9]H. F. Arellano, F. A. Brieva, and W. G. Love, Phys. Rev. Lett. **63**, 605 (1989).

[10]R. Machleidt, K. Holinde, and Ch. Elster, Phys. Rep. **149**, 1 (1987).

[11]A. K. Kerman, H. McManus, and R. M. Thaler, Ann. Phys. **8**, 551 (1959).

[12]K. M. Watson, Phys. Rev. **89**, 575 (1953).

[13]A. L. Fetter and K. M. Watson, in *Advances in Theoretical Physics,* edited by K. A. Brueckner (Academic, New York, 1965), Vol. 1.

[14]G. Takeda and K. M. Watson, Phys. Rev. **97**, 1336 (1955).

[15]J. S. Bell and E. J. Squires, Phys. Rev. Lett. **3**, 96 (1959).

[16]H. Feshbach, Ann. Phys. (N.Y.) **5**, 357 (1958); **19**, 287 (1962).

[17]P. B. Jones, *The Optical Model in Nuclear and Particle Physics* (Wiley, New York, 1963).

[18]J. Hüfner and C. Mahaux, Ann. Phys. **73**, 525 (1972).

[19]W. G. Love, Phys. Rev. C **20**, 1638 (1979).

[20]M. Lacombe, B. Loiseau, J. M. Richard, R. Vinh Mau, J. Côté, P. Pirès, and R. de Tourreil, Phys. Rev. C **21**, 861 (1980).

[21]J. M. J. van Leewen and A. S. Reiner, Physica **27**, 99 (1961).

[22]H. F. Arellano, M. S. thesis, Universidad de Chile, 1984 (unpublished).

[23]K. Amos, L. Berge, F. A. Brieva, A. Katsogiannis, L. Petris, and L. Rikus, Phys. Rev. C **37**, 934 (1988).

[24]C. M. Vincent and S. C. Phatak, Phys. Rev. C **10**, 391 (1974), and references therein.

[25]A. Picklesimer, P. C. Tandy, R. M. Thaler, and D. H. Wolfe, Phys. Rev. C **30**, 1861 (1984).

[26]R. A. Eisenstein and Frank Tabakin, Phys. Rev. C **26**, 1 (1982).

[27]J. J. Kelly *et al.*, Phys. Rev. C **39**, 1222 (1989).

[28]E. J. Stephenson, J. Phys. Soc. Jpn. (Suppl.) **55**, 316 (1985).

[29]E. Bleszynski *et al.*, Phys. Rev. C **37**, 1527 (1988).

[30]D. A. Hutcheon *et al.*, Nucl. Phys. **A483**, 429 (1988); P. Schwandt, private communication.

[31]A. Rahbar *et al.*, Phys. Rev. Lett. **47**, 1811 (1981).

[32]Ch. Elster and P. C. Tandy, Phys. Rev. C **40**, 881 (1989).

[33]Ch. Elster, Taksu Cheon, Edward Redish, and P. C. Tandy, Phys. Rev. C **41**, 814 (1990).